Tigilanol tiglate is an oncolytic small molecule that induces immunogenic cell death and enhances the response of both target and non-injected tumors to immune checkpoint blockade

Jason K Cullen [1,2,3] Pei-Yi Yap,[1] Blake Ferguson,[1] Zara C Bruce,[1] Motoko Koyama,[1] Herlina Handoko,[1] Kevin Hendrawan,[1] Jacinta L Simmons,[1,2] Kelly M Brooks,[1] Jenny Johns,[1] Emily S Wilson,[1] Marjorie M A de Souza,[1] Natasa Broit,[1] Praphaporn Stewart,[4] Daniel Shelley,[4] Tracey McMahon,[4] Steven M Ogbourne,[3,4] Tam Hong Nguyen,[1] Yi Chieh Lim,[5] Alberto Pagani,[6] Giovanni Appendino,[6] Victoria A Gordon,[3] Paul W Reddell,[3] Glen M Boyle,[1,2] Peter G Parsons[1,3]

For numbered affiliations see end of article.

Correspondence to
Dr Jason K Cullen;
Jason.Cullen@qbiotics.com

ABSTRACT

Background Tigilanol tiglate (TT) is a protein kinase C (PKC)/C1 domain activator currently being developed as an intralesional agent for the treatment of various (sub) cutaneous malignancies. Previous work has shown that intratumoral (I.T.) injection of TT causes vascular disruption with concomitant tumor ablation in several preclinical models of cancer, in addition to various (sub)cutaneous tumors presenting in the veterinary clinic. TT has completed Phase I dose escalation trials, with some patients showing signs of abscopal effects. However, the exact molecular details underpinning its mechanism of action (MoA), together with its immunotherapeutic potential in oncology remain unclear.

Methods A combination of microscopy, luciferase assays, immunofluorescence, immunoblotting, subcellular fractionation, intracellular ATP assays, phagocytosis assays and mixed lymphocyte reactions were used to probe the MoA of TT in vitro. In vivo studies with TT used MM649 xenograft, CT-26 and immune checkpoint inhibitor refractory B16-F10-OVA tumor bearing mice, the latter with or without anti-programmed cell death 1 (PD-1)/anti-cytotoxic T-lymphocyte-associated protein 4 (CTLA-4) mAb treatment. The effect of TT at injected and non-injected tumors was also assessed.

Results Here, we show that TT induces the death of endothelial and cancer cells at therapeutically relevant concentrations via a caspase/gasdermin E-dependent pyroptopic pathway. At therapeutic doses, our data demonstrate that TT acts as a lipotoxin, binding to and promoting mitochondrial/endoplasmic reticulum (ER) dysfunction (leading to unfolded protein response[mt/ER] upregulation) with subsequent ATP depletion, organelle swelling, caspase activation, gasdermin E cleavage and induction of terminal necrosis. Consistent with binding to ER membranes, we found that TT treatment promoted activation of the integrated stress response together with the release/ externalization of damage-associated molecular patterns (HMGB1, ATP, calreticulin) from cancer cells in vitro and in vivo, characteristics indicative of immunogenic cell death (ICD).

WHAT IS ALREADY KNOWN ON THIS TOPIC

⇒ Tigilanol tiglate (TT) is a protein kinase C (PKC) activator that has previously been shown to ablate tumors, in part via vascular disruption. Additional work with inhibitors and PKC-inactive analogs of TT has suggested that PKC activation plays a role in the efficacy of this compound.

Confirmation of ICD in vivo was obtained through vaccination and rechallenge experiments using CT-26 colon carcinoma tumor bearing mice. Furthermore, TT also reduced tumor volume, induced immune cell infiltration, as well as improved survival in B16-F10-OVA tumor bearing mice when combined with immune checkpoint blockade.

Conclusions These data demonstrate that TT is an oncolytic small molecule with multiple targets and confirms that cell death induced by this compound has the potential to augment antitumor responses to immunotherapy.

BACKGROUND

Injectable and localized therapeutics for the treatment of cancer are becoming more widely used in clinical practice as direct debulking agents and/or adjuvants to other modalities, including immune checkpoint inhibitor therapy.[1–3] While oncolytic viruses containing immunological payloads have garnered much attention,[4–6] I.T. (intratumoral) administration of immunostimulatory monoclonal antibodies, cytokine preparations, pattern recognition receptor agonists, immune cells and several small molecule drugs are also being investigated in this space.[7–15] One of these agents, tigilanol tiglate

---

WHAT THIS STUDY ADDS

⇒ Our study sheds further light on the mechanism of action of TT and uncovers a previously unappreciated immunomodulatory role for this compound in the oncological space. Specifically, we show that TT also has PKC-independent effects in the context of tumor ablation. Our data are consistent with TT causing unresolved endoplasmic reticulum stress in endothelial and cancer cells at therapeutically administered doses, leading to the initiation of cell death signaling that culminates in the activation of gasdermin E dependent pyroptosis in these cell types. At subcytotoxic concentrations, TT can also induce NF-κB transcriptional responses in cancer cells, together with promoting the secretion of various chemotactic cytokines/chemokines responsible for immune cell recruitment. In vitro and in vivo studies demonstrate that the pyroptosis induced by TT is immunogenic (through promoting the release/externalization of damage associated molecular patterns) and can promote the development of a systemic antitumor immune response. Furthermore, in addition to promoting the recruitment of T cells to injected lesions, we show that TT combines with immune checkpoint inhibitor (ICI) therapy to restrict the recurrence of injected lesions in an ICI-resistant tumor model, and can also inhibit the growth of non-injected lesions. In both scenarios, combination treatment improved survival outcomes.

HOW THIS STUDY MIGHT AFFECT RESEARCH, PRACTICE OR POLICY

⇒ These findings suggest that TT acts via multiple pathways to promote tumor ablation and may also effectively control disease burden in the right (immunogenic) tumor and patient context. In addition, TT may also help augment the benefits of immunotherapy in clinical practice, especially in patients who do not initially respond to checkpoint inhibition.

(TT; also known as EBC-46), belongs to a family of naturally derived epoxytigliane esters with anticancer properties that activate members of the protein kinase C (PKC) family of serine/threonine kinases.[16 17] Given structural similarities with the phorbol esters, TT is believed to act as a diacylglycerol (DAG) mimetic and thus has the potential to activate other C1 domain containing proteins.[18] Previous studies have shown that a single I.T. dose of TT can induce tumor ablation in several mouse models of cancer, in addition to various skin tumors in client owned companion animals.[16 19 20] A field efficacy study in canines has demonstrated that TT delivered I.T. is effective at curing cutaneous mast cell tumors in >75% of patients, an outcome that led to the approval of TT (marketed as STELFONTA) as a veterinary medicine in Australia, the European Union and the USA.[21]

TT directed tumor ablation is thought to occur primarily as a result of vascular disruption and extensive hemorrhagic necrosis at the injection site.[16] Further work using pharmacological inhibition demonstrated a partial requirement for PKC-based signaling in drug efficacy in vivo. Importantly, we have also shown that "PKC-inactive" analogs of TT fail to completely destroy tumors, suggesting that PKC/C1 domain signaling may be important for efficacy.[17] A Phase I dose-escalation trial of TT in humans (ACTRN12614000685617) has shown strong evidence of anticancer efficacy and signs of abscopal effects in some patients.[22] However, the underlying mechanism of action responsible for the antitumor efficacy of TT, together with its immunomodulatory potential in the oncological context remains poorly understood.

Here, we show that TT, in addition to causing localized tumor destruction, can promote the development of a systemic antitumor immune response, including improving both target and non-injected tumor responses to immune checkpoint blockade. TT treatment may therefore have both local and systemic effects in the context of cancer therapy, and may also improve the clinical responses of refractory tumors to immune checkpoint therapy.

RESULTS

TT rapidly ablates melanoma xenograft tumors in a concentration dependent manner

We first performed a dose-response study in a xenograft model of human melanoma (MM649 human melanoma cells) to understand what concentrations of TT were required for effective tumor ablation. We assumed that TT was diluted twofold when injected into tumors (50 µL drug into a ~100 mm³ tumor) and that the drug would be homogenously distributed through the entire tumor volume. We subsequently found that I.T. doses of TT lower than 15 µg (266 µM or 27 nmole) were less efficacious at promoting tumor ablation (figure 1A). While partial ablation of the tumor site was observed with 7.5 µg (133 µM or 13.5 nmole) of the drug, tumors soon recurred at the edge of the primary lesion, suggesting that I.T. concentrations >133 µM/13.5 nmole were required for full efficacy in this model. To understand how TT acts at the cellular level in this context we modeled both tumor (MM649) and its associated vasculature (2H-11—SV40 immortalized murine endothelial cells) in vitro and determined the effects of therapeutically relevant doses of drug on cell morphology/survival over 12 hours. At these concentrations, TT induced a rapid necrosis in both cell lines as indicated by propidium iodide (PI) staining (figure 1B, C and online supplemental movie S1, S2). Morphologically, cells appeared to detach from the well surface and swell, forming a "halo"—like structure during the course of PI uptake. As expected, the kinetics of this cell death process were dose-dependent, with death occurring more rapidly at higher concentrations of TT (figure 1B, C). At subefficacious in vivo doses i.e. 100 µM, cell survival was minimally affected over the time course. PKC inhibition with BIS-1 had minimal effects on cell survival in MM649 and 2H-11 cells treated with either 500 or 300 µM TT, suggesting that cell death was largely PKC-independent in this context (figure 1D, E). Identical morphological changes to those seen in MM649 and 2H-11 cells were also observed in a larger panel of squamous cell carcinoma/melanoma cell lines cultured in two or three-dimensions and treated with both 300 and 500 µM TT, that is, cell
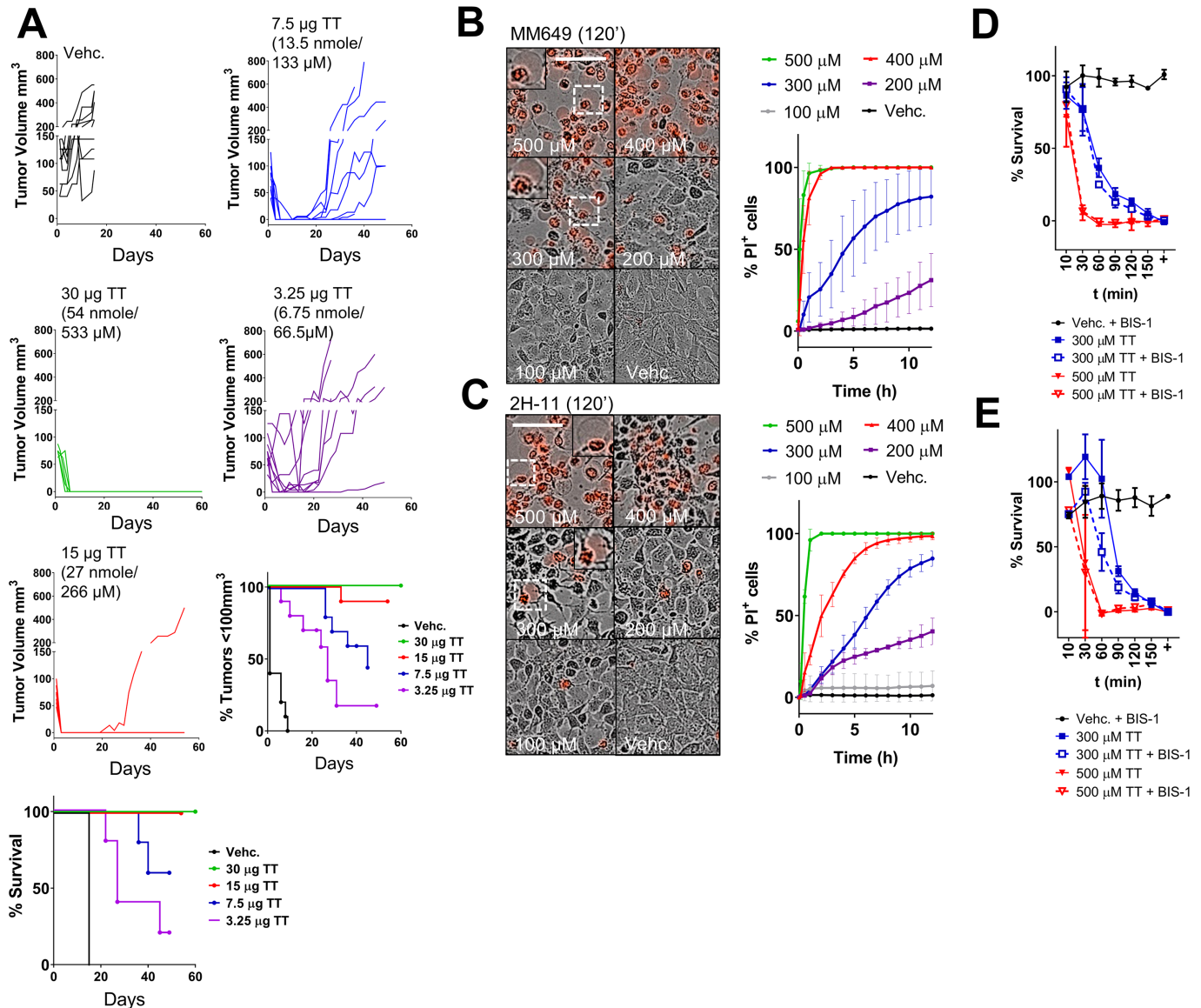
Figure 1 Dose-response experiments in vivo indicate that high concentrations of tigilanol tiglate (TT) are required for therapeutic efficacy. (A) High concentrations of TT are required for efficacy in a human melanoma xenograft model. Established MM649 tumors in BALB/c *Foxn1^nu* nude mice were injected intratumorally with various concentrations of TT (50 µL) and tumor volume measured versus time. Tumor volume graphs, together with Kaplan-Meier analysis (% tumors <100 mm³) are depicted. n=6–10 tumors per concentration tested. Overall mouse survival is also shown. Both vehicle and 15 µg TT (27 nmole/266 µM) data sets were previously published in (*19*) and are reproduced here. (B, C) TT induces a dose-dependent disruption of plasma membrane integrity in tumor/endothelial cell lines at therapeutically relevant concentrations. MM649 (human melanoma) (B) and 2H-11 (immortalized mouse endothelial) (C) cells were incubated with various concentrations of TT or vehicle (Vehc.) in media containing 2 µg/mL PI. Images were acquired over time using an Incucyte. The percentage of PI+ve cells was determined per field of view over time ± SD. Boxes show cells undergoing cell swelling and necrosis. n=3. Scale bars: 100 µm. (D, E) Inhibition of PKC has minimal effects on MM649 (D) and 2H-11 (E) cell survival in response to TT treatment at therapeutically relevant doses. Cells in 96-well plate format were pre-incubated ± 5 µM BIS-1, after which they were treated with either 500 or 300 µM TT for the indicated times. BIS-1 remained on all wells for 24 hours. Cell survival was determined via MTS assay after 24 hours and compared with untreated controls. +: both compound and inhibitor remained on cells for 24 hours. Mean cell survival ± SD. is shown. n=3. Statistical analysis by two-way ANOVA with Sidak's correction. Comparisons made between TT and TT + BIS-1 samples. *p<0.05, **p<0.01, ***p<0.001, ****p<0.0001. ANOVA, analysis of variance; PI, propidium iodide; PKC, protein kinase C; TT, tigilanol tiglate.

rounding and cytoplasmic swelling (online supplemental figure 1).

Although the cell death induced in vitro by TT appeared to be PKC-independent, our previous studies have suggested that TT-directed PKC/C1 domain activation plays a role in treatment efficacy in vivo. To investigate this further we repeated experiments with an inactive analog of TT (EBC-158) that is unable to activate PKC.[17] We found that although EBC-158 could induce cell swelling and necrosis at therapeutically

relevant concentrations in tumor and endothelial cells in vitro, the kinetics of this process were significantly delayed compared with TT (online supplemental figure 2). Consistent with previous studies we found that unlike TT, EBC-158 was not efficacious at inducing tumor ablation in vivo at $15\,\mu g$ ($258\,\mu M$ or $26\,nmole$), suggesting that PKC/C1 domain activation plays a role in drug response in vivo (online supplemental figure 2A). Interestingly, we saw that tumors still underwent partial hemorrhagic necrosis after EBC-158 administration (online supplemental figure 2B), consistent with our in vitro data. Together, these results suggest that PKC/C1 domain activity, although not strictly necessary for inducing cell swelling and necrosis, may modulate the kinetics of this process, and may thus play a role in TT-directed tumor ablation.

TT induces a dose-dependent pyroptosis involving activation of the intrinsic/extrinsic pathways of apoptosis and GSDME cleavage

We next investigated the effects of TT on mitochondrial function in MM649 and A-431 (human SCC) cells in vitro. Here, we found that TT induced loss of mitochondrial membrane potential ($\Delta\Psi_m$) around 10–30 min post administration, dependent on dose (figure 2A, online supplemental movie S3, S4). We subsequently found that drug administration led to the release of mitochondrial cytochrome c either concomitantly with ($500\,\mu M$ TT) or soon after ($300\,\mu M$ TT) loss of TMRM staining in HeLa cells expressing cytochrome c-EGFP, demonstrating that drug-induced loss of $\Delta\Psi_m$ culminated in mitochondrial outer membrane permeabilization (MOMP; online supplemental figure 3A,B and online supplemental movie S5). Further experimentation in MM649 cells expressing Tom20-mEmerald revealed that mitochondrial swelling also occurred after TT-induced loss of TMRM staining at both 500 and $300\,\mu M$ (approximately 30–40 min post initial administration of compound; online supplemental figure 3C,D). This progressed to an increase in Tom20-mEmerald signal in large vacuolar type structures that also stained positive for LysoTracker Deep Red (online supplemental figure 3E, F and online supplemental movie S6), indicative of an increase in mitophagy. As expected, mitochondrial swelling and induction of mitophagy occurred at later time points in cells treated with $300\,\mu M$ TT and was not as extensive as observed with $500\,\mu M$ of the compound. Together, these data demonstrated that TT promotes loss of $\Delta\Psi_m$, followed by mitochondrial swelling, MOMP and the upregulation of mitochondrial degradation prior to cell death, the kinetics of which ultimately depended on TT dose.

Consistent with the mitochondrial swelling, further interrogation of our live cell imaging showed that loss of $\Delta\Psi_m$ was followed by vacuolization of the cytosol at both concentrations of the drug tested (figure 2A, white dashed boxes). This rapidly progressed to the cytoplasmic swelling and necrosis (figure 2A, red dashed boxes) we had previously observed in our Incucyte-based assays.

Similar swollen, vacuolar structures were also seen in toluidine blue stained sections of MM649 cells treated with TT at both $300\,\mu M$ and $500\,\mu M$ (figure 2B). Luminescence-based assays also revealed that TT induced a rapid and significant reduction in intracellular ATP levels in both A-431 and MM649 cells, the kinetics of which were dependent on treatment dose (figure 2C). Furthermore, lactate dehydrogenase (LDH) release assays confirmed concomitant plasma membrane rupture in both cell lines (figure 2D). TT-induced cell death could also be significantly delayed at both concentrations through the use of a chloride channel blocker and TRPM4 inhibitor, NPPB and 9-phenanthrol, suggesting that loss of cell viability in response to drug may also involve an ion channel/TRPM4-based mechanism (online supplemental figure 4 A,B).

While cytoplasmic swelling/necrosis predominated in drug treated cells, at $300\,\mu M$ TT membrane blebbing was especially apparent in both cell types prior to plasma membrane rupture (figure 2A, white arrows). Interestingly, the large majority of nuclei treated with $500\,\mu M$ TT remained intact, while nuclear fragmentation or shrinking was extensively observed with $300\,\mu M$ TT (figure 2A, red dashed boxes). This suggested that apoptotic-based pathways were active or had time to proceed at lower doses of drug. Consistent with this, we observed caspase-8, caspase-9, caspase-3, caspase-7, Bid and poly (ADP-ribose) polymerase (PARP) cleavage in response to TT at 300 and $500\,\mu M$ treatment in both cell types with slightly different kinetics (figure 2E and online supplemental figure 4C). While differences were found between cell types in terms of caspase/Bid/PARP cleavage, drug treatment consistently led to Mcl-1 downregulation in both MM649 and A-431 cells at $500\,\mu M$ and $300\,\mu M$ (online supplemental figure 4C). Consistent with the induction of cytoplasmic swelling and necrosis, we also found that the pore forming protein GSDME was cleaved and activated (N-terminal 45 KDa fragment) during TT-mediated cell death. Neither MLKL phosphorylation or activating cleavage of GSDMD were observed after TT administration, suggesting that TT does not promote necroptosis or gasdermin D-dependent pyroptosis (figure 2E). Use of a pan-caspase inhibitor (Q-VD-OPh) prior to the administration of TT also had some inhibitory activity in MM649 cells at $300\,\mu M$ (online supplemental figure 4D). Manipulating components of the intrinsic apoptotic machinery that act at or adjacent to mitochondria also protected cells to some extent from TT treatment. Indeed, overexpression of Bcl-2 in HeLa cells or deletion of *Apaf1* in MEFs protected cells from both $300\,\mu M$ and $500\,\mu M$ TT (online supplemental figure 4 E,F). In contrast, deletion of Bax and/or Bak in MEFs appeared to protect cells to a significant extent from $300\,\mu M$ but not $500\,\mu M$ TT (online supplemental figure 4F). Consistent with a role for caspase activation and GSDME cleavage in TT-mediated pyroptosis, CRISPR mediated knockout of GSDME, caspase 3/caspase 7 and caspase 3/caspase 7/GSDME protected cells from both $300\,\mu M$ and $500\,\mu M$ TT (figure 2F), although this was
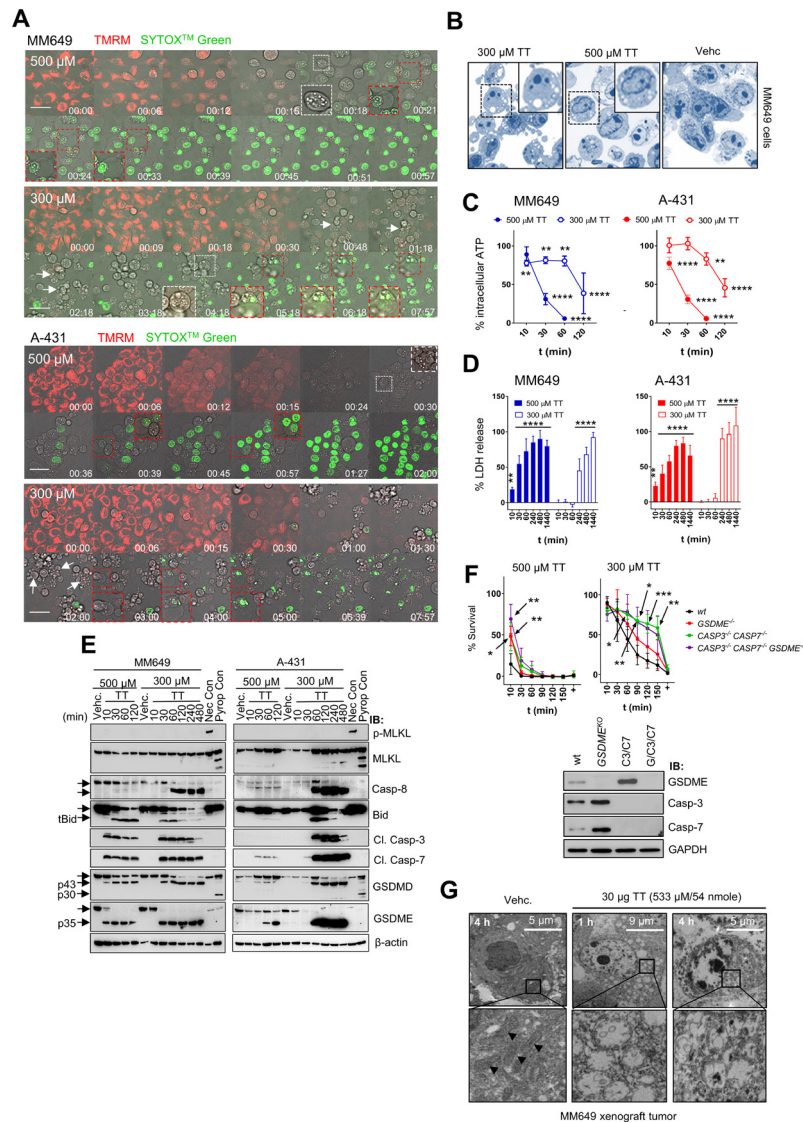
Figure 2 Therapeutically relevant concentrations of TT induce mitochondrial dysfunction, pyroptosis and terminal necrosis in vitro and in vivo. (A) Loss of mitochondrial membrane potential ($\Delta\Psi_m$) and cytoplasmic vacuolization occur prior to cell swelling and plasma membrane rupture in TT-treated cells. MM649 and A-431 cells were incubated with media containing 20 nM TMRM (red) and 50 nM SYTOX™ Green (green). Treated cells were subsequently imaged at different time points using confocal spinning disk fluorescence microscopy. White boxes: cells showing cytoplasmic vacuolization. Red boxes: cells showing plasma membrane swelling prior to lysis. White arrow heads: membrane blebbing. 60×mag. Scale bars: 20 µm. Note the presence of DNA fragmentation in 300 µM treated MM649 and A-431. (B) TT induces the formation of intracellular vacuoles. MM649 cells were treated with TT at the indicated concentrations for 1 hour and stained with toluidine blue prior to fixation and sectioning. 100×mag. (C, D) Reduction in intracellular ATP levels occurs prior to lysis (LDH release) in TT treated cells. A-431 and MM649 cells plated in 96-well plate format were treated with 300 or 500 µM TT. At distinct time points, intracellular ATP levels (C) or extracellular LDH release (D) were determined. Mean values ± SD are plotted in each graph. n=3. Statistical analysis by two-way ANOVA with Dunnett's correction. Comparisons to vehicle treated controls. *p<0.05, **p<0.01, ***p<0.001, ****p<0.0001. (E) Analysis of cell death pathway induced in response to 500 and 300 µM TT. WCE obtained at the indicated time points from MM649 and A-431 cells were separated by SDS-PAGE and transferred to nitrocellulose in preparation for immunoblotting. Immunoblotting was performed with the indicated antibodies. Arrows indicate full-length protein or processed fragments. tBid=truncated and active Bid fragment. GSDMD: p43 is inactive while p30 is active. GSDME: p35 is active. (F) Knockout of *GSDME, CASP3 and CASP7* protects cells from both 300 and 500 µM TT. Knockout (KO) cells plated in 96-well plate format were treated with either 500 or 300 µM TT for the indicated times. % cell survival was determined via MTS assay after 24 hours and compared with untreated controls. +: TT remained on cells for 24 hours. Mean % cell survival ± SD is shown. n=4. The lower panel shows immunoblotting analysis of KO cell lines with the indicated antibodies. Statistical analysis by two-way ANOVA with Dunnet's correction. Comparisons made to wt treated controls. *p<0.05, **p<0.01, ***p<0.001, ****p<0.0001. (G) Intratumoral injection of TT gives rise to similar morphological changes, including the formation of intracellular vacuoles, in MM649 tumor cells in vivo. MM649 xenograft tumors established in BALB/c *Foxn1^nu* nude mice were treated with TT and then fixed in preparation for TEM analysis. ANOVA, analysis of variance; ATP, adenosine triphosphate; LDH, lactate dehydrogenase; TEM, transmission electron microscopy; TT, tigilanol tiglate; WCE, whole cell extract; wt, wild-type.

transient at 500 µM TT. Together, these data demonstrate that therapeutically relevant concentrations of TT induce a caspase-dependent pyroptosis involving GSDME pore formation in cells.

To understand whether a similar morphological response occurred in vivo after TT administration, that is, the appearance of swollen vacuolar structures followed by cell necrosis, we also treated MM649 tumors in nude mice with TT and prepared samples for electron microscopy. Indeed, we observed similar morphological characteristics in vivo after injection of TT (30 µg or 533 µM) (figure 2G), indicating that our in vitro studies held relevance for drug response in vivo.

TT binds to endoplasmic reticulum membranes and promotes the activation of mitochondrial/endoplasmic reticulum stress responses

As TT likely acts as a DAG mimetic, we hypothesized that it might induce pyroptosis and terminal necrosis in a manner independent of PKC/C1 domains by binding to and perturbing the function of organellular membranes. To investigate this, we took advantage of a fluorescent analog with physiochemical and biological properties similar to those of TT (known as TT-A). Due to the known interplay between mitochondria and the endoplasmic reticulum (ER) in cell physiology and the fact that mitochondrial function was affected, we decided to overexpress fluorescently tagged mitochondrial and ER resident proteins (Tom20-mEmerald and Sec61-RFP) to identify colocalization with TT-A by fluorescence microscopy. As expected, TT-A (300 µM) rapidly accumulated into membrane structures including both mitochondria and ER, 10 min after addition (figure 3A,B and online supplemental movie S7). At later time points (40–70 min), we observed the formation of globular structures containing TT-A which did not co-localize with either Tom20-GFP or Sec61-RFP but appeared to co-localize with lysosomal structures as indicated by LysoTracker Deep Red staining (figure 3 C,D and online supplemental movie S8), consistent with induction of a lysosome mediated degradation pathway. TT-A induced cell death also occurred approximately 1–2 hours after treatment with this concentration of drug. In contrast to TT-A, TT (300 µM) appeared to accumulate predominantly in ER membranes after 15 min rather than mitochondria (figure 3E). Strikingly, we also observed a large amount of TT in the "cytosolic" fraction. Immunoblotting suggested that this fraction was heavily contaminated with ER membranes. However, given we had previously seen TT-A form droplet-like structures after administration, we reasoned that TT may also be processed into lipid droplets. Indeed, it is well known that ER components (including protein disulphide isomerase - PDI) are frequent contaminants in these preparations.[23 24] Furthermore, due to the buoyancy of lipid droplets, they are not removed from crude cytoplasmic extracts during the high-speed centrifugation step required for ER isolation. Consistent with this hypothesis, we found that TT induced the formation of lipid droplet structures in MM649 cells as indicated by Nile red staining (online supplemental figure 5A). Thus, TT accumulates in ER membranes and is possibly processed into lipid droplet-like structures that undergo attempted breakdown via a lysosomal-based pathway.

Given that TT bound to ER membranes, we investigated whether stress signaling pathways associated with this organelle were activated. Treatment of MM649 cells with 500 µM TT led to the rapid phosphorylation (t=10 min) of Ire1α, PERK, PKR, p38 and JNK1/2, indicative of activation of the ER/mitochondrial unfolded protein response (UPR$^{ER/mt}$) and stimulation of stress kinase signaling (figure 3F). Consistent with this, we also found that eiF2α was rapidly phosphorylated in response to TT, demonstrating rapid activation of the integrated stress response (ISR) (figure 3F). A similar outcome was observed in cells treated with 300 µM TT, although activation of p38 and PKR occurred at later time points and was maintained for at least 120 min. The change in PERK migration due to phosphorylation was confirmed through the use of PhosTag and phosphatase-based experiments (figure 3F, online supplemental figure 5 B,C). Inhibition of Ire1α (kinase and RNase inhibition with Kira6) but not PERK, significantly protected cells from lower doses of TT (figure 3 G,H). Bcl-2, in addition to inhibiting Bax/Bak-dependent MOMP, has also recently been shown to inhibit Ire1 and as a result facilitate tissue homeostasis.[25] This might also help explain why Bcl-2 overexpression protects cells against TT-induced pyroptosis (online supplemental figure 4E). Thus, TT binding to ER membranes induces upregulation of UPR$^{mt/ER}$ signaling, ISR induction and promotion of a cell death pathway that may involve Ire1α activation.

TT promotes the release/externalization of damage associated molecular patterns from cancer cells

As we had observed both caspase-8 activation and ISR induction following TT treatment, we reasoned that TT may promote immunogenic cell death (ICD) during the transition to pyroptosis/necrosis. We therefore analyzed additional markers of ICD in TT-treated cells, including the generation of reactive oxygen species (ROS), ATP release, calreticulin externalization, HMGB1 release and type I interferon (IFN) production.[26] In addition, we also investigated whether TT could induce activation of nuclear factor kappa B (NF-κB) dependent responses given that these have also been associated with the immunogenicity of cell death. We found that TT stimulated a significant increase in ROS production over time in response to 300 µM of drug in both MM649 and A-431 cells (figure 4A). Drug exposure also induced extracellular ATP release in a dose-dependent manner from both MM649 and A-431 cells (t$_{max}$=10–30 min (500 µM) and 60 min (300 µM); figure 4B), which appeared to occur in concert with plasma membrane disruption (figure 4C) suggesting that it occurred postmortem. ELISA assays demonstrated that HMGB1 release, while low, was significant in both A-431 and MM649 cells at later time points
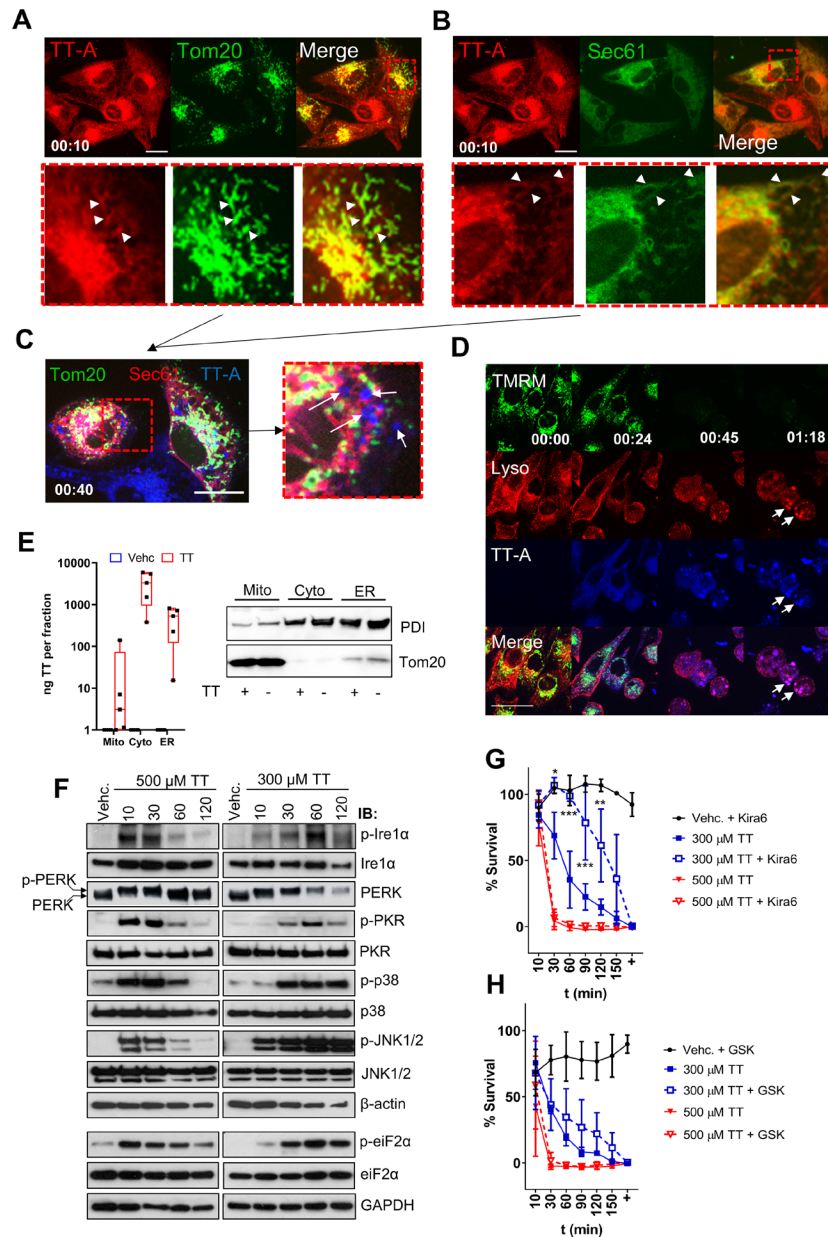
Figure 3 TT binds to ER membranes and induces activation of mitochondrial/ER stress signaling and the integrated stress response. (A, B, C, D) A fluorescent TT analog, TT-A, initially binds to mitochondrial/ER membranes (t=10 min) but accumulates in lysosomes at later time points (t=40+ min). MM649 cells overexpressing mEmerald-Tom20 and mCherry-Sec61 beta were incubated with 300 µM TT-A, then visualized via spinning disk confocal microscopy. Mitochondrial (A) and ER (B) based colocalization with TT-A can be observed after 10 min (white arrow heads). At later time points, TT-A accumulates in structures that do not colocalize with mitochondrial/ER markers, but localize in lysosomes (C and D). In (D) MM649 cells were stained with 100 nM LysoTracker Deep Red and 20 nM TMRM prior to incubation with TT-A. Images were acquired using a spinning disk confocal microscope. 60×mag. In (C) white arrows show TT-A with no colocalization with mitochondrial/ER markers. In (D) white arrows show colocalization between TT-A and LysoTracker Deep Red. Scale bars in (A–D) 20 µm. (E) TT accumulates in ER. MM649 cells treated with vehicle/300 µM TT and isolated after 30 min were subjected to subcellular fractionation and HPLC-MS analysis. The median concentration values of TT acquired in each compartment are shown in box plot format. n=4. Mitochondrial (Tom20) and ER (PDI) markers were used to assess the purity of subcellular fractions via immunoblotting (lower panel). (F) TT induces ER stress and activation of the integrated stress response. MM649 cells were treated with the indicated concentrations of TT and WCE generated at distinct time points. Protein (30 µg) was separated via SDS-PAGE and immunoblotting performed with the indicated antibodies. Arrows indicate differentially migrating species. (G, H) Inhibition of Ire1α, but not PERK, protects cells from lower doses of TT. Cells in 96-well plate format were incubated ± 5 µM Kira6 (G) or 5 µM GSK2606414 (GSK: H) for 1 hour prior to incubation with 500/300 µM TT for the indicated times. Cell survival was determined via MTS assay after 24 hours and compared with untreated controls. +: compound and inhibitor remained on cells for 24 hours. Mean cell survival ± SD is plotted in each graph. n=3. Statistical analysis by two-way ANOVA with Sidak's correction. Comparisons were made between TT and TT + Kira6/GSK samples. *p<0.05, **p<0.01, ***p<0.001, ****p<0.0001. ANOVA, analysis of variance; PDI, protein disulphide isomerase; ER, endoplasmic reticulum; TT, tigilanol tiglate; WCE, whole cell extract.
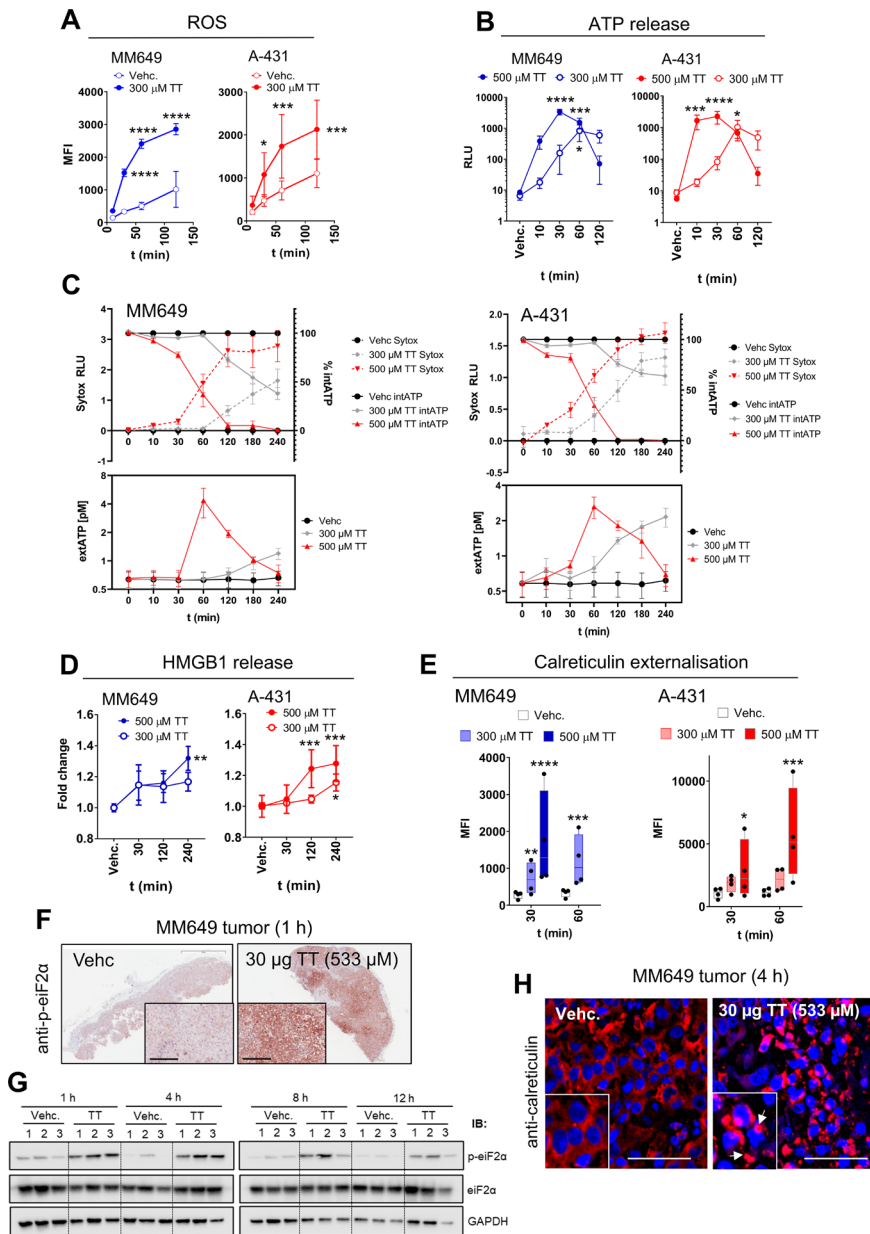
Figure 4 TT induces biomarkers of immunogenic cell death in vitro and in vivo. (A) TT promotes ROS production in MM649 and A-431 cells. Cells stained with 5 ng/mL DHE were incubated with 300 µM TT for the indicated times and analyzed by flow cytometry. Mean fluorescence intensity (MFI) values are shown ± SD. n=4. (B) TT promotes extracellular ATP release. Cells were treated with TT (300/500 µM) for the indicated time periods and cell culture supernatants analyzed for ATP content. Mean relative luminescence units (RLU) are shown ± SD. n=4. (C) TT-induced ATP release occurs concomitantly with plasma membrane disruption. Again, MM649 and A-431 cells were treated with TT and the levels of intracellular (intATP) and extracellular (extATP) determined over time, together with plasma membrane breakage via SYTOX™ Green uptake (SYTOX). n=4. (D) TT promotes HMGB1 release. Cells were treated with TT (300/500 µM) for the indicated time periods and cell culture supernatants analyzed for HMGB1 content via ELISA. Mean fold change values (compared with vehicle treated controls) are shown ± SD. n=4. (E) TT promotes calreticulin externalization prior to membrane rupture. Cells were treated with TT (300/500 µM) for the indicated time periods and subsequently incubated with LIVE/DEAD far red prior to staining for cell surface calreticulin. Cells were analyzed via flow cytometry. MFI values in box plot format are shown for each graph. n=4. (F, G) Treatment of tumors with TT results in eiF2α phosphorylation in vivo. Tumors (75–100 mm³; three tumors per condition) treated with vehicle or 30 µg (533 µM/54 nmole) TT I.T. and isolated after 1 hour for immunohistochemistry (F) or over a 1–12 hours time course for immunoblotting (G) (30 µg protein) with anti-phospho-eiF2α and total eiF2α. Scale bar: 200 µm. (H) TT promotes calreticulin externalization in vivo. MM649 tumors (75–100 mm³) were treated with vehicle or 30 µg (54 nmole) TT I.T. and isolated after 4 hours. Representative image from 4 hours treated sample. n=2. Scale bar: 50 µm. Statistical analysis by two-way ANOVA with Sidak's correction in (A) and Dunnett's correction in (B, E). A mixed effects analysis with Dunnett's correction was performed for data in (D). Comparisons were made to vehicle-treated controls in all cases. *p<0.05, **p<0.01, ***p<0.001, ****p<0.0001. ANOVA, analysis of variance; DHE, dihydroethidium; I.T., intratumoral; ROS, reactive oxygen species; TT, tigilanol tiglate.

(figure 4D). Flow cytometry also revealed that drug treatment induced significant calreticulin externalization in both cell types (figure 4E). Use of an NF-κB luciferase reporter system[17] demonstrated that while TT could induce upregulation of NF-κB mediated transcription in HeLa cells at lower concentrations (50–100 μM), this did not occur in MM649 and A-431 cells (online supplemental figure 6A,B,C). Furthermore, although we observed TT-induced secretion of interleukin (IL)-6, IL-8, CXCL9 and CXCL10 in some cell lines at lower concentrations of drug (50–100 μM), we failed to see evidence of bona fide STING activation in response to TT as indicated by a lack of type I IFN secretion (online supplemental figure 6D,E,F). Consistent with the induction of ICD in vitro, we also observed eiF2α phosphorylation and the formation of calreticulin puncta in MM649 human melanoma xenografts treated with TT, suggesting that ICD also occurred in vivo (figure 4F, G, H). Similar or improved responses were observed in the mouse melanoma line, B16-F10-OVA (online supplemental figure 7).

TT promotes the development of T-cell directed antitumor responses in vitro and in vivo

To determine whether the death induced by TT was immunogenic, we first performed co-culture experiments in which drug-treated cancer cells (B16-F10-OVA) pre-stained with 5-chloromethylfluorescein diacetate (CMFDA) were incubated with immature bone marrow derived cells (BMDCs) isolated from C57BL/6J mice. Flow cytometry indicated that drug-treated cells were phagocytosed effectively by CD11c$^+$ cells, the extent of which was dependent on drug concentration and treatment time (figure 5A and B). Imaging of several CD11c$^+$CMFDA^{mid} cells from the 500 μM TT treatment sample confirmed antigenic uptake, as indicated by the presence of intracellular green puncta (figure 5C; white arrowheads).

Given the uptake by immature BMDCs, we next investigated whether drug could help promote the activation of antigen-specific T-cell responses in vitro (see online supplemental figure 8 for gating strategy). Consistent with our previous results, we found that prior treatment of B16-F10-OVA cells with TT led to significant activation and proliferation of both OVA-directed CD4 and CD8 T cells when combined with BMDCs in mixed lymphocyte reaction assays, as indicated by carboxyfluorescein succinimidyl ester (CFSE) dilution and CD69 upregulation (increase in CD69$^+$ prolif$_{pos}$ and CD69$^-$ prolif$_{pos}$ cells; figure 5D). Incubation of BMDCs with B16-F10-OVA cells that had undergone freeze thaw cycles failed to activate CD4/CD8 T-cell responses, and the removal of BMDCs from TT-treated samples also led to a similar result (figure 5D). Thus, TT-mediated cell death in cancer cells promotes the development of antigen-specific T-cell responses in vitro.

To test whether TT promoted ICD in vivo, we performed additional experiments using the immunogenic CT-26 colon carcinoma model. Two CT-26 tumors (75–100 mm^3) were implanted via subcutaneous (s.c.) injection in the flanks of immunocompetent *BALB/c* mice and treated I.T. with either vehicle or 7.5, 15 or 30 μg TT. Tumors that recurred before day 10 in the TT-treated cohorts were reinjected with drug. 20 days after the initial treatment, cured mice were reinjected with CT-26 cells at a spatially distinct site to determine whether a bona fide antitumor immune response had been generated (figure 6A). In contrast to I.T. injection of vehicle, administration of TT ablated 73–83% of CT-26 tumors over a broad concentration range (figure 6B and C). While all tumors initially responded to treatment, a small fraction recurred at the edge of the lesion site (figure 6B). In the 15 μg and 7.5 μg TT treatment groups, 2 and 7 tumors were re-treated, respectively. Interestingly, drug efficacy was largely comparable among the concentrations of TT tested under these conditions, although less tumors ultimately recurred at 30 μg (five tumors) compared with 15 and 7.5 μg TT (eight tumors). Remarkably, I.T. treatment efficacy was significantly reduced when similar experiments were performed in nude mice (figure 6C, online supplemental figure 9A), demonstrating a requirement for T cells to prevent tumor recurrence. Consistent with the in vitro data, we also found that prior treatment with TT protected immunocompetent (figure 6D, E) but not nude (figure 6E, online supplemental figure 9B) mice from rechallenge with the same cell line. Experiments using AH1 directed tetramers, splenocytes and IFN-γ staining also confirmed that TT promoted the development of functional, AH-1 specific T cells in these mice (figure 6F, G). We also performed a gold standard vaccination assay to determine whether TT acted as a true ICD inducer. Here, we found that mock injection (phosphate-buffered saline (PBS)) or vaccination of mice with CT-26 cells that had undergone prior freeze-thaw (F/T) cycles failed to protect these mice against rechallenge with live cancer cells (online supplemental figure 10): 15/15 tumors growing in PBS-treated mice and 10/15 tumors growing in F/T treated mice). Furthermore, protection against rechallenge was not observed in mice vaccinated with CT-26 cells treated with 150 μM TT (13/15 tumors developed after rechallenge). Conversely, vaccination of mice with cells that had been treated with either doxorubicin or 300/500 μM TT protected mice against subsequent injection of live CT-26 cells (online supplemental figure 10): 0/15 and 4/15 tumors growing in 300 μM and 500 μM TT-treated mice, respectively). However, we found that several tumors formed at the vaccination site in mice administered 300/500 μM TT-treated cells, indicating that a population of cells could recover from TT treatment under these conditions. Although this was so, the fact that tumor growth was significantly inhibited on the rechallenge site by vaccination with TT-treated cells suggest that TT is a bona fide ICD-inducing agent.

TT promotes T-cell infiltration into tumors

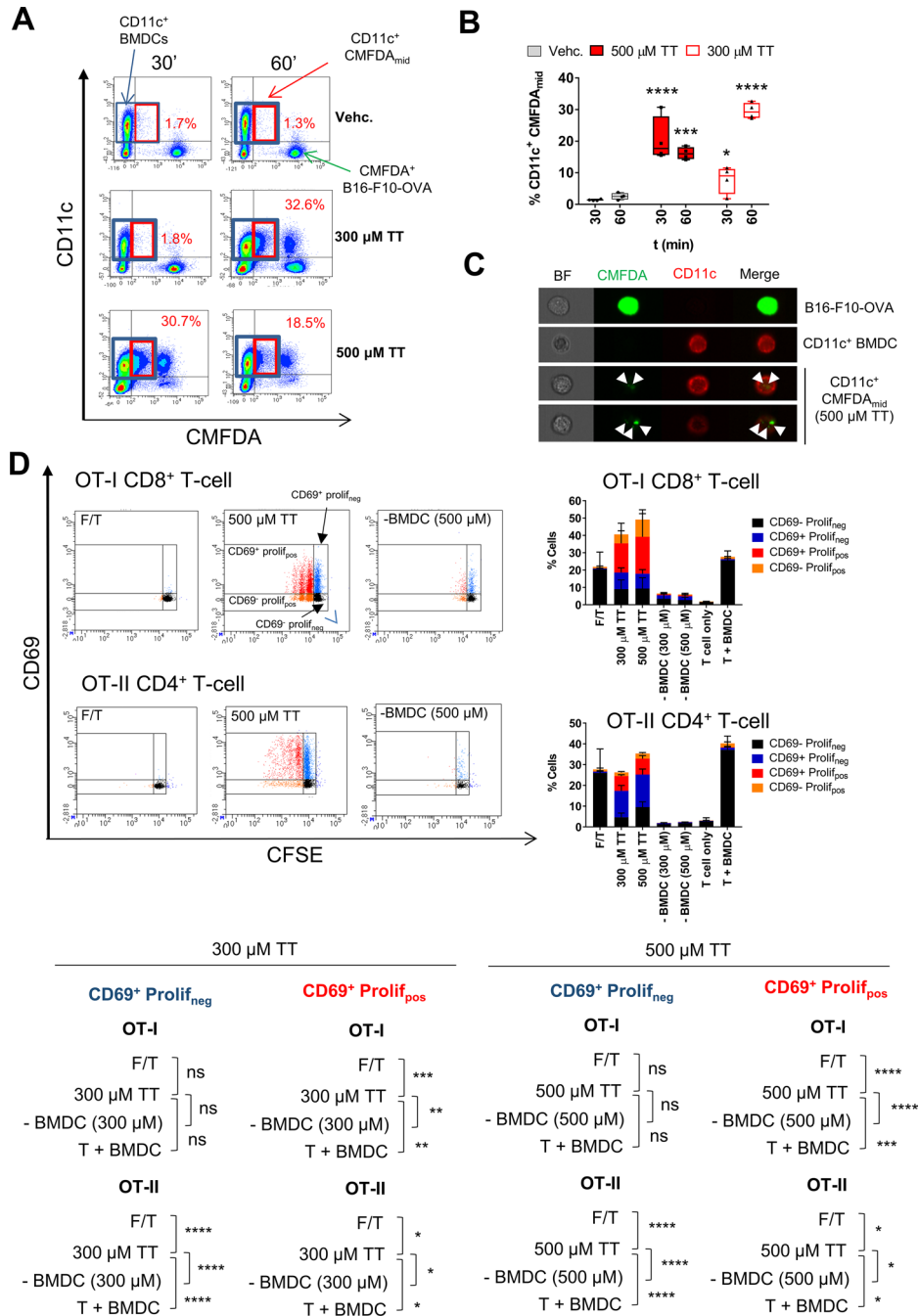We next sought to understand whether TT could promote damage associated molecular pattern (DAMP) release

Figure 5 TT-directed pyroptosis is immunogenic in vitro. (A, B, C) TT-treated B16-F10-OVA cells are effectively phagocytosed by immature BMDCs in vitro. TT-treated B16-F10-OVA cells (pre-stained with CMFDA) were incubated with immature BMDCs for 4 hours, stained with anti-CD11c-APC and then subsequently analyzed via flow cytometry (A). Blue boxes: CD11c+ve cells with/without CMFDA uptake. Red boxes: CD11c+CMFDA$_{mid}$ cells, that is, cells that have phagocytosed dying cancer cell fragments. Median % CD11c+CMFDA$_{mid}$ cells observed for each treatment were plotted via box plot format (B). n=4. CD11c+CMFDA$_{mid}$ cells were also imaged to confirm antigenic uptake (C). White arrows indicate intracellular CMFDA-stained fragments. Statistical analysis by two-way ANOVA with Dunnett's correction. Comparisons were made to vehicle treated controls. (D) TT-treated B16-F10-OVA cells can promote the activation/proliferation of OVA-directed CD4 and CD8 T-cell responses in vitro. BMDCs from PTPRCA mice (CD45.1$^+$CD45.2$^-$) pre-incubated with TT treated cells (16 hours) were co-incubated with CFSE stained T cells from OT-I (CD8$^+$Va2$^+$Vb5$^+$ T cells from CD45.1$^-$CD45.2$^+$ mice) and OT-II (CD4$^+$Va2$^+$Vb5$^+$ T cells from CD45.1$^-$CD45.2$^+$ mice) mice. Early activation (anti-CD69) and proliferation (CFSE dilution) markers were assessed in live cells at t=2 (OT-I) or 4 (OT-II) days via flow cytometry. The % of non-activated (CD69$^-$ Prolif$_{neg}$), early activated (CD69$^+$ Prolif$_{neg}$), activated (CD69$^+$ Prolif$_{pos}$) and late activated (CD69$^-$ Prolif$_{pos}$) T cells±SD are depicted in each graph. n=3. Statistical analysis by two-way ANOVA with Tukey's correction. See comparisons below main graphs for statistical data. *p<0.05, **p<0.01, ***p<0.001, ****p<0.0001. ANOVA, analysis of variance; BMDC, bone marrow derived cells; CFSE, carboxyfluorescein succinimidyl ester; CMDFA, 5-chloromethylfluorescein diacetate; TT, tigilanol tiglate.
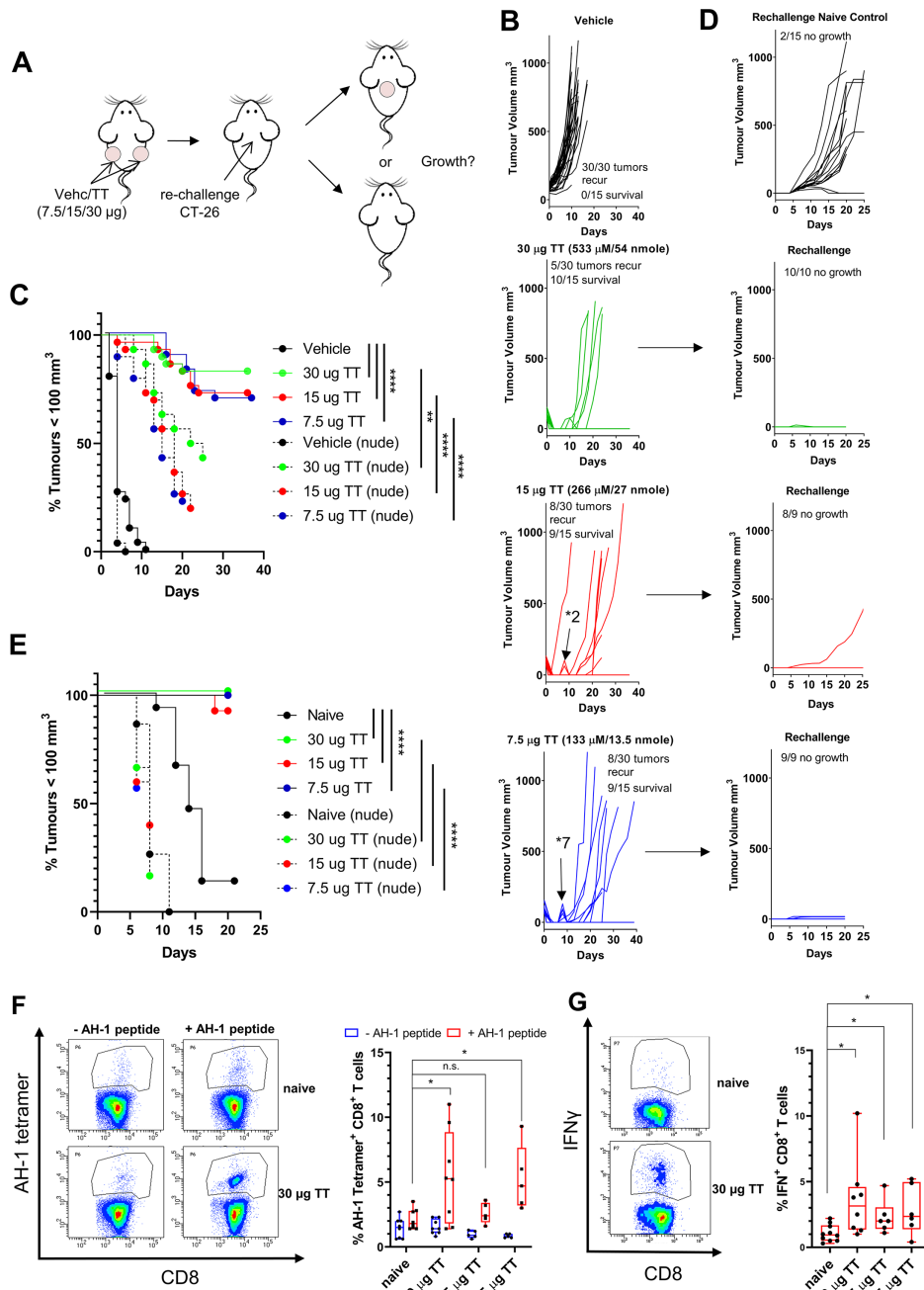
Figure 6 TT promotes the development of T-cell dependent antitumor immunity in vivo. (A) Schematic diagram of experimental design. BALB/c mice with CT-26 tumors were treated with TT, allowed to resolve and cured mice rechallenged with CT-26 cells. (B) TT ablates CT-26 tumors in BALB/c immunocompetent mice. Mice with two distinct CT-26 tumors were injected with the indicated concentrations of TT. 15 mice per condition, n=30 tumors per group. *Indicates number of tumors reinjected with TT. (C) T cells are required to prevent the relapse of TT-injected tumors in immunocompetent mice. Kaplan-Meier analysis of individual CT-26 tumors (% tumors <100 mm^3) in immunocompetent and immunodeficient (nude) mice injected with the indicated concentrations of TT. Data acquired from tumor growth curves detailed in (B) and in online supplemental figure 9A (immunodeficient (nude) mice). Statistical analysis by log-rank (Mantel-Cox) test. (D, E) TT promotes the development of antitumor immunity. Naïve and TT-cured mice were rechallenged with CT-26 cells. Tumor growth curves are depicted for each condition (D). Vehicle: n=15 mice. 30 µg TT: n=10 cured mice. 15 µg and 7.5 µg TT: n=9 cured mice. Kaplan-Meier analysis of data acquired in (D) is shown in (E) together with data acquired from experiments in nude mice (see online supplemental figure 9B). Statistical analysis by log-rank (Mantel-Cox) test. (F, G) TT treatment leads to the development of tumor-directed T cells in the periphery. Splenocytes isolated from naïve and rechallenged mice detailed in (D) were incubated with AH-1 peptide, stained with AH-1 directed tetramers (F) or anti-IFN-γ (G) together with LIVE/DEAD Aqua, anti-CD3, CD4, CD8 and analyzed via flow cytometry. Representative flow cytometry dot plots, together with box plots (median values) of replicate data (% AH-1 tetramer+ CD8+ or % IFN-γ+ CD8+ T cells) are shown. Vehicle: n=9; 30 µg TT: n=8; 15 µg and 7.5 µg TT: n=6. Statistical analysis by Student's t-test. *p<0.05, **p<0.01, ***p<0.001, ****p<0.0001. IFN, interferon; TT, tigilanol tiglate.

and T-cell recruitment to tumors in a "cold", immune checkpoint inhibitor (ICI)-refractory tumor model of melanoma. To investigate this, B16-F10-OVA cells were implanted s.c. into C57BL/6 mice (two tumors per mouse) and treated with either vehicle or 15 µg TT once they reached 200 mm³. Remnant tumors were isolated on Days 1 and 4 post I.T. injection (online supplemental figure 11A). Immunohistochemistry and immunofluorescence revealed that TT induced significant loss of nuclear HMGB1 staining, together with punctate calreticulin staining indicative of membrane externalization within tumors 24 hours post-treatment that was not observed with vehicle treatment (online supplemental figure 11B,C). Treatment with TT also leads to significant recruitment of CD3$^+$ cells into these tumors at day 4 (online supplemental figure 11D,E). Although there was a marked increase in CD8$^+$ T cells in this scenario, the large majority of CD3$^+$ cells at this time point appeared to be CD4$^+$ cells (online supplemental figure 11F,G).

Combination of TT with immune checkpoint therapy improves therapeutic outcomes

We next sought to understand whether TT could improve the efficacy of checkpoint inhibition (anti-programmed cell death 1 (PD-1)/anti-cytotoxic T-lymphocyte-associated protein 4 (CTLA-4) therapy) in the B16-F10-OVA model. A schematic of the treatment protocol can be seen in figure 7A. Again, B16-F10-OVA cells were implanted s.c. into C57BL/6 mice (two tumors per mouse) and IgG, anti-PD-1, anti-CTLA-4 or a combination of the two administered 2 days prior to I.T. injection of vehicle or TT into both target lesions (30 and 15 µg TT). Antibody was subsequently administered every 2 days for a further three cycles. B16-F10-OVA tumors were non-responsive to anti-PD-1, anti-CTLA-4 or anti-PD-1/CTLA-4 combination therapy (with I.T. injection of vehicle) as previously observed by others.[27] Similar to our prior experiments, tumors were significantly responsive to I.T. injection of both 15 and 30 µg TT+IgG compared with both IgG+vehicle and anti-PD-1+vehicle, anti-CTLA-4+vehicle and anti-PD-1/anti-CTLA-4+vehicle treatments. However, ≥45% of treated lesions recurred in these mice around 10–30 days post-treatment (figure 7B, C; online supplemental figure 12). While combination treatment with 15 µg TT and anti-CTLA-4 had a substantial but ultimately non-significant effect on tumor recurrence and mouse survival, combination of TT at this dose with anti-PD-1 or anti-PD-1/anti-CTLA-4 had no additive effect compared with treatment with 15 µg of TT alone (figure 7B). However, the use of 30 µg TT in combination with anti-PD-1 led to less tumor recurrence and improved overall survival compared with 30 µg TT alone (figure 7C; online supplemental figure 12B). A similar but statistically significant outcome was observed in anti-PD-1/CTLA-4 combination experiments (figure 7C; online supplemental figure 12C). These data suggest that immune checkpoint therapy can combine effectively with TT to improve anticancer responses, prevent tumor recurrence and improve survival.

To further investigate the potential of checkpoint inhibitor/TT combinations in this model, we performed an experiment to understand whether immune checkpoint therapy, together with I.T. administration of TT to a single target tumor could affect the growth of non-injected lesions (anenestic response). Tumors were generated as above and IgG, anti-PD-1, anti-CTLA-4 or a combination administered 2 days prior to I.T. injection of vehicle/TT into one tumor (30 and 15 µg TT). Again, checkpoint inhibitor/s were administered for a further three cycles every 2 days (figure 7D). As expected, TT-injected tumors (+ IgG only) were significantly ablated at both 15 and 30 µg TT, in contrast to vehicle treated lesions (figure 7E, F; online supplemental figure 13; "Injected" panels). A significant or almost significant change in the growth of non-injected B16-F10-OVA lesions and subsequent survival was observed in anti-CTLA-4+TT and anti-PD-1/CTLA-4+TT combinations only (at both 15 and 30 µg TT), when compared with either anti-CTLA-4+vehicle, anti-PD-1/CTLA-4+vehicle or IgG+TT-treated mice (figure 7E, F; online supplemental figure 13; "Non-injected" panels). Thus, anti-CTLA-4 or anti-PD-1/CTLA-4 combination immunotherapy improves the response of non-injected lesions to TT treatment and leads to increased survival.

DISCUSSION

While PKC/C1 domain activation is believed to play a role in the anticancer efficacy of TT, an in-depth understanding of its mechanism of action has remained elusive. Here, we show that in addition to activating PKC/C1 domain containing species, TT induces cell death directly at therapeutically relevant concentrations via a pyroptopic-based mechanism that is largely PKC-independent. TT likely promotes this mechanism of cell destruction by acting as a lipotoxin, subsequently binding to and inducing mitochondrial/ER dysfunction in a variety of cell types, including neoplastic and associated endothelial cells. This ultimately leads to the activation of mitochondrial/ER stress response pathways, ATP depletion, activation/cleavage of caspases and gasdermin E, the opening of ion channels (TRPM4?), organelle/cell swelling and subsequent plasma membrane rupture. Importantly, dying cancer cells treated with TT release DAMPs that are capable of inducing antigen specific immune responses in vitro and in vivo. Together with data showing that TT can promote the recruitment of tumor infiltrating lymphocytes (TILs) and improve the efficacy of immune checkpoint inhibition in an ICI-refractory model of mouse melanoma, these results suggest that TT directed tumor debulking can remodel the tumor microenvironment in addition to stimulating the immune system. Thus, it appears that TT may have effects on multiple targets in the context of tumor ablation and immune modulation. A model depicting these results can be seen in online supplemental figure 14.

There are a number of observations reported in this study that support these conclusions. First, we found via
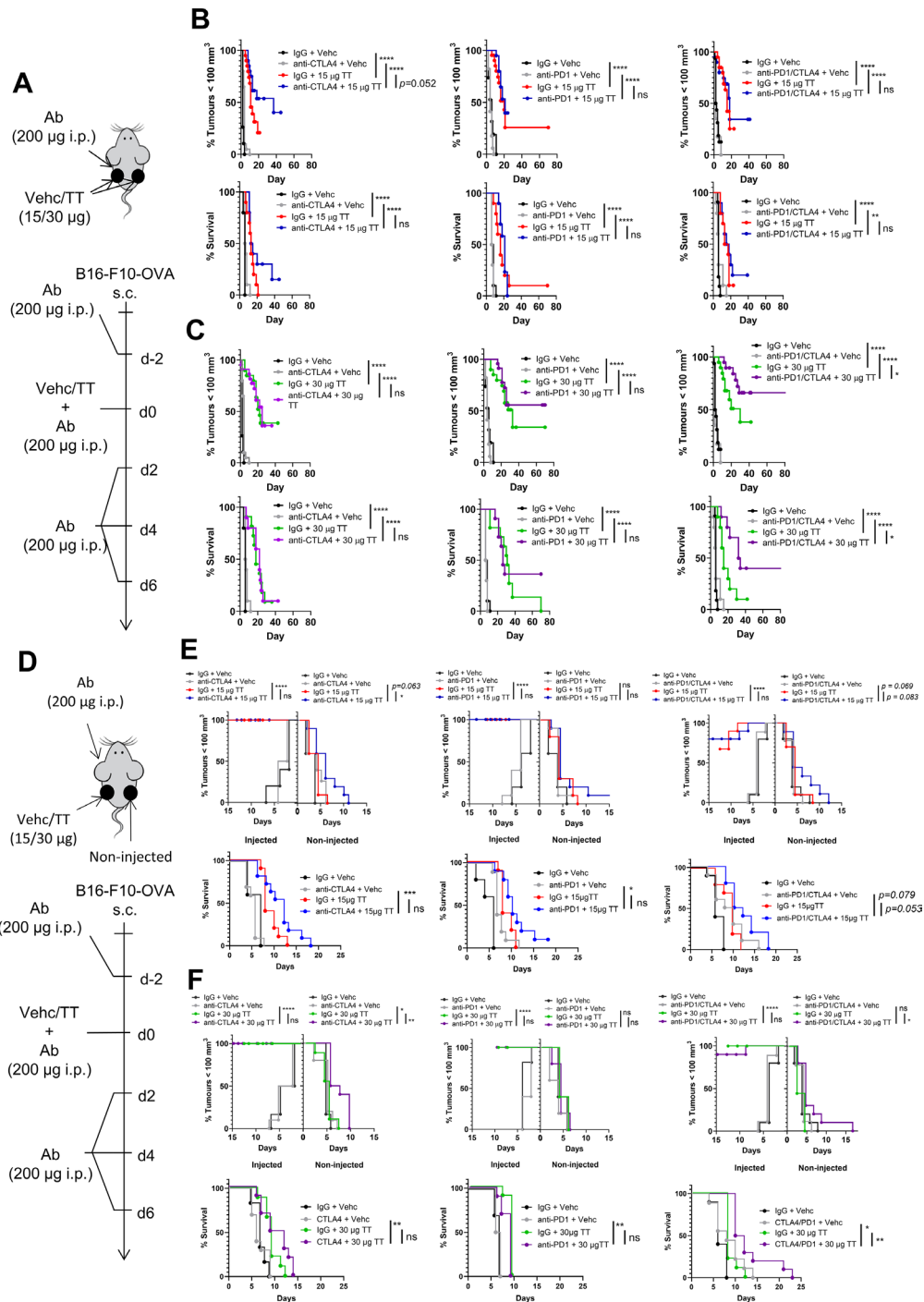
Figure 7 TT combines with immune checkpoint inhibitor therapy to improve antitumor responses in an immune checkpoint inhibitor-refractory model of melanoma. (A) Schematic of the dual treatment regime. Mice with two distinct B16-F10-OVA tumors on their hindquarters were administered IgG/anti-PD-1/anti-CTLA-4 or a combination thereof via i.p. injection prior to I.T. injection of both tumors with vehicle or TT (15/30 µg). Mice received antibody every 2 days after I.T. injection for a further three cycles. (B, C) TT combines with checkpoint inhibitors to prevent tumor recurrence and improve overall survival. Kaplan-Meier analysis of individual tumors <100 mm³ (upper panels) and overall mouse survival (lower panels). n=20 tumors treated per condition. 10 mice per condition. (D) Schematic of the abscopal treatment regime. Mice with two distinct B16-F10-OVA tumors on their hindquarters were administered IgG/anti-PD-1/anti-CTLA-4 or a combination thereof via i.p. injection prior to I.T. injection of a single tumor with vehicle or TT (15/30 µg). Mice received antibody every 2 days after I.T. injection for a further three cycles. (E, F) TT combines with anti-CTLA-4 and anti-CTLA-4/PD-1 to inhibit the growth of non-injected B16-F10-OVA tumors and improve mouse survival. Kaplan-Meier analysis of individual tumors <100 mm³ and of mouse survival. n=10 mice per condition, except for 15 µg TT anti-IgG+vehicle (anti-CTLA-4 and anti-PD-1 cohorts) and 30 µg TT anti-IgG+vehicle (anti-CTLA-4 cohort) where n=5–6. Statistical analysis by log-rank (Mantel-Cox) test. *p<0.05, **p<0.01, ***p<0.001, ****p<0.0001.CTLA-4, cytotoxic T-lymphocyte-associated protein 4; i.p, intraperitoneal; I.T., intratumoral; PD-1, programmed cell death 1; TT, tigilanol tiglate.

a combination of microscopy, cell subfractionation and mass spectrometry (MS)-based experimentation that TT rapidly accumulates in ER membranes after administration. Activation of UPR$^{mt/ER}$ follows this binding (10 or 30 min, dependent on concentration), as indicated by phosphorylation of Ire1α/PERK and PKR, integral components of the mammalian UPR$^{ER/mt}$ [28 29]. Consistent with this observation, our data also demonstrate that JNK1/2 and p38, downstream targets of Ire1α/PERK/PKR,[30 31] were rapidly activated after the addition of TT (10 min at 500 μM). Ire1α/PERK/PKR/JNK/p38-based stress signaling pathways have been shown to have protective or pro-death roles in cells, dependent on both the strength and duration of the stress stimulus.[32] How does TT disrupt mitochondrial/ER function to promote this sequence of events? It is possible that TT may do this via the activation of PKC/C1 domain containing proteins or the activation/inhibition of other targets at the ER membrane. Indeed, a structurally-related PKC activator, ingenol mebutate, has been shown to interact with various ER and mitochondrial proteins with downstream effects on mitochondrial function.[33] However, as relatively high concentrations of the drug are required for the induction of cell death (>100 μM in vitro), a more reasonable explanation may be that after TT accumulates in ER it has detrimental effects on membrane structure/homeostasis which result in the activation of stress signaling pathways (UPR^{ER}) that ultimately promote cell death due to the unresolved nature of the chemical stress. While primarily involved in sensing proteotoxic stress, recent studies have shown that both Ire1α and PERK can sense lipid saturation and structural perturbation at the ER membrane.[34 35] Interestingly, activation of PKR (an ER and mitochondrial-associated stress kinase) has also been associated with cellular responses to harmful lipids.[36] Ire1 activation in response to lipotoxicity induced by palmitate has also recently been shown to promote a rapid, XBP1-independent cell death in cardiomyocytes, paralleling our observations here.[37] A role for Ire1α is also consistent with our data which demonstrated that pharmacological inhibition of Ire1α can protect cells from lower concentrations of TT.

Presumably, Ire1α/PERK/PKR/JNK/p38 signaling is first activated in an attempt to protect the cell from TT mediated lipotoxicity, an attempt which ultimately fails and results in progression towards cell death. Consistent with this, previous reports have shown that ER stress mediated induction of autophagy is dependent on Ire1α-JNK-Beclin1 signaling.[38] In addition, PKR is known to upregulate autophagy in response to the fatty acid palmitate in vivo.[39] The fact that TT-A and TT are processed into lipid droplet-like structures and targeted for lysosomal mediated degradation also corroborates with this hypothesis. JNK and p38 are known to modulate the activity/stability of both pro-apoptotic and anti-apoptotic Bcl-2 family members that play key roles in MOMP induction, cytochrome *c* release and cell survival.[40 41] Indeed, JNK and GSK3 are known to phosphorylate Mcl-1 and

stimulate its degradation,[42] the latter phenomenon being observed in our studies.

Paralleling MOMP induction and cytochrome *c* release, we also observed activation of the apoptotic machinery (caspase-3/7/8/9, Bid and PARP cleavage, as early as 10–30 min) in response to drug, in addition to GSDME cleavage that may be partially responsible for the cellular swelling and terminal necrosis observed in response to drug. Inhibition of the intrinsic pathway of apoptosis (pharmacologically and genetically) had a significant effect on cell survival at both 300 and 500 μM TT, although inhibition was only transient. A similar result was observed in CASP-3/CASP-7/GSDME knockout cells. Presumably, the nature of the unresolved stress causes the activation of an alternative regulated cell death pathway/s in the absence of caspase/GSDME activation over longer treatment periods, a scenario that has been observed extensively in functional studies investigating cell death mechanisms.[43]

Organellular swelling and necrosis were also observed in in vivo tumors, confirming physiological relevance. Destruction of both tumor cells and their associated endothelium via this mechanism (together with PKC/C1 domain activation) may help account for the hemorrhagic necrosis that has been observed in mouse, veterinary and human tumors after I.T. injection of TT.[16] This is also in line with our previous observations, which have shown tumor cell necrosis and complete loss of vascular (CD31) staining in TT treated tumors at later time points (4 hours).[16] Interestingly, the pyroptosis seen in vitro can be inhibited to some extent at both 300 and 500 μM TT by the ion channel inhibitors NPPB and 9-phenathrol. It is tempting to speculate that these inhibitors, in addition to inhibiting chloride channels and the non-selective transmembrane cation channel TRPM4, respectively, may also inhibit GSDME pores. However, TRPM4 opening is also known to promote Na$^+$ influx, leading to loss of osmotic balance and terminal necrosis in several cell types, including endothelial cells.[44] TRPM4 has also been shown to play a role in promoting immunogenic necrosis in response to treatment with various therapeutics (ErSO, BHPI, LTX-315) that induce UPR^{ER} activation and release of Ca^{2+} from the ER.[45] Interestingly, PKC activation has also been shown to increase the sensitivity of TRPM4 to Ca^{2+}-dependent opening.[46] This might help explain why "PKC-inactive" analogs of TT, for example, EBC-158 and EBC-211,[17] do not induce pyroptosis with the same kinetics as TT. Proteomic analysis of GSDME also suggests that it is phosphorylated at several sites that might control its pore forming function. Further experiments will be required to understand whether TT-directed PKC/C1 domain activation plays a role in modulating ion channel/TRPM4/gasdermin E-dependent cell death outcomes and thus the efficacy of TT in vivo.

Our data also demonstrate that TT can stimulate anti-tumor immune cell responses, both in vitro and in vivo. This may occur via the induction of ICD in tumor cells, although it is possible that residual TT may also have

PKC-dependent effects on stromal and/or immune cell subsets at the tumor periphery or once such cell types have been recruited to treated lesions. Indeed, we found that TT stimulates IL-6, IL-8, CXCL9 and CXCL10 secretion from cancer cells, cytokines/chemokines with roles in promoting immune cell recruitment. Low concentrations of TT that enter systemic circulation after I.T. injection may also affect the activity of stromal and/or immune cells in non-injected tumors. Consistent with our cancer cell data, TT is known to induce pro-inflammatory responses in keratinocytes, fibroblasts and peripheral blood mononuclear cell (PBMC) preparations, and can activate PKC isoforms essential to T and natural killer (NK) cell function and survival.[17] A structurally distinct PKC activator, ingenol mebutate, has also recently been shown to reactivate hypofunctional T cells, suggesting that TT might also be capable of stimulating exhausted TILs in the tumor microenvironment.[47] Consistent with ICD induction after treatment, we observed ATP release, calreticulin exposure and HMGB1 release from cancer cell lines in response to therapeutically relevant concentrations of TT, again dependent on cell type. Other characteristics of ICD, including caspase-8 activation, ER stress and eIF2α phosphorylation were also observed in vitro after treatment.[26 48] However, we failed to see any evidence of STING pathway activation in vitro. We did observe phosphorylation of eIF2α and calreticulin processing consistently in MM649 tumors treated with TT, as was HMGB1 loss and calreticulin externalization in B16-F10-OVA tumors, demonstrating DAMP release/externalization in vivo. Rechallenge experiments in CT-26 bearing mice and the identification of tumor specific T cells via tetramer analysis after TT treatment corroborated with these observations and demonstrated that TT is a bona fide ICD inducing agent. This was partially confirmed by vaccination experiments. Indeed, although we saw protection against rechallenge in the large majority of mice vaccinated with TT-treated cells in vitro, we observed substantial growth of tumors at the vaccination site. This is a similar situation to that observed with cardiac glycosides[49] and underlies the technically challenging aspect of these experiments, which may be due in part to the rapid nature of the pyroptosis induced by TT (figure 1B, C and figure 2A).

Interestingly, in addition to being required to reject tumor implantation at a spatially distinct site to the I.T. injection, T cells were also required to prevent tumor recurrence at the TT treatment site in this model. This is consistent with our observations that TT promotes T-cell recruitment to tumors (see below). Thus, in the right (immunogenic) tumor and patient context, TT monotherapy may effectively control disease burden. Signs of this were observed in early safety trials with TT, where two patients with melanoma experienced abscopal responses to non-injected tumors after IT injection.[22]

Finally, our data indicate that TT works in combination with immune checkpoint blockade to (1) prevent the recurrence of ICI-refractory tumors after I.T. injection

and (2) restrict tumor growth at non-injected sites. As alluded to above, we first demonstrated that TT could promote significant T-cell infiltration into remnant tumor mass, indicating that drug may turn "cold" tumors "hot", thus priming them for further immunotherapy. This data is consistent not only with the ability of TT to induce ICD, but also with its ability to upregulate the secretion of various chemotactic cytokines/chemokines (IL-6, IL-8, CXCL9 and CXCL10) from cancer cells that play roles in recruiting innate and adaptive immune cells. Following these findings, we observed combinatorial responses at the level of tumor recurrence and mouse survival with both anti-PD-1 and anti-PD-1/anti-CTLA-4 combination therapy when all tumors were injected with TT (in contrast to TT treatment alone). Combinatorial activity was only observed at the highest dose of TT tested in the B16-F10-OVA model (30 μg), suggesting some form of concentration dependence that may be related to the underlying mechanism of cell death induced by TT. Interestingly, more favorable abscopal responses in non-injected tumors were observed when TT was combined with anti-CTLA-4 therapy rather than anti-PD-1, although we also observed more robust responses in the anti-PD-1/CTLA-4 combination. Given that the 9H10 clone is known to deplete regulatory T cells (Tregs), it is tempting to speculate that this cell type may inhibit abscopal responses after TT injection. Interestingly, recent evidence in mouse models of triple-negative breast cancer (resistant to checkpoint blockade) has shown that administration of LTX-315 (an ICD inducing agent), together with radiotherapy and anti-CTLA-4 antibody leads to the control of untreated/metastatic lesions in an NK cell dependent manner.[50] Given the low expression of major histocompatibility complex-I in the B16-F10 line and its insensitivity to immune checkpoint therapy,[27] it is possible that innate lymphocyte subsets may also play a role in TT-directed efficacy in non-injected tumors when combined with anti-CTLA-4, or even injected tumors in the presence of anti-PD-1/anti-CTLA-4. Together, these data suggest that TT may aid cancer patients who do not respond initially to checkpoint inhibition, and may therefore help augment the benefits of immunotherapy.

TT is currently being evaluated in several clinical trials based on this and other data, including a Phase IB/IIA trial in head and neck squamous cell carcinoma (NCT05608876) and a Phase IIA trial in soft tissue sarcomas (NCT05755113). Further preclinical work will be needed to understand how dose/scheduling affects antitumor activity and how these parameters can be modulated with additional immunotherapeutic strategies to improve outcomes with TT in human patients.

Methods
See "online supplemental information" for details on the methodology used in this study.

All animal procedures were approved in accordance with NHMRC guidelines (Australian Code for the Care and Use of Animals for Scientific Purposes eighth Edition,

Author affiliations
[1]QIMR Berghofer Medical Research Institute, Herston, Queensland, Australia
[2]The University of Queensland, Brisbane, Queensland, Australia
[3]QBiotics Group Limited, Brisbane, Queensland, Australia
[4]University of the Sunshine Coast, Maroochydore DC, Queensland, Australia
[5]Danish Cancer Society Research Centre, Copenhagen DK, Denmark
[6]Dipartimento di Scienze del Farmaco, Università Degli Studi del Piemonte Orientale, Novara, Italy

Patient consent for publication Not applicable.

Ethics approval Not applicable.

Provenance and peer review Not commissioned; externally peer reviewed.

Data availability statement Data are available upon reasonable request. All data relevant to the study are included in the article or uploaded as supplementary information. All data generated and analyzed during this study are contained within the published article and its Supplementary Information file. All materials are available on reasonable request and negotiation of an MTA with QBiotics Group Ltd.

ORCID iD
Jason K Cullen http://orcid.org/0000-0003-4961-1673

REFERENCES

1. Goldberg EP, Hadba AR, Almond BA, et al. Intratumoral cancer chemotherapy and Immunotherapy: opportunities for nonsystemic preoperative drug delivery. *J Pharm Pharmacol* 2010;54:159–80.
2. Chua CYX, Ho J, Demaria S, et al. Emerging technologies for local cancer treatment. *Adv Ther (Weinh)* 2020;3.
3. Melero I, Castanon E, Alvarez M, et al. Intratumoural administration and tumour tissue targeting of cancer Immunotherapies. *Nat Rev Clin Oncol* 2021;18:558–76.
4. Andtbacka RHI, Collichio F, Harrington KJ, et al. Final analyses of optim: a randomized phase iii trial of talimogene laherparepvec versus granulocyte-macrophage colony-stimulating factor in unresectable stage III–IV melanoma. *J Immunother Cancer* 2019;7:145.
5. Heo J, Reid T, Ruo L, et al. Randomized dose-finding clinical trial of oncolytic immunotherapeutic vaccinia JX-594 in liver cancer. *Nat Med* 2013;19:329–36.
6. Lang FF, Conrad C, Gomez-Manzano C, et al. Phase I study of DNX-2401 (Delta-24-RGD) oncolytic adenovirus: replication and immunotherapeutic effects in recurrent malignant glioma. *J Clin Oncol* 2018;36:1419–27.
7. Schwarze JK, Duerinck J, Dufait I, et al. A phase I clinical trial on Intratumoral and intracavitary administration of ipilimumab and nivolumab in patients with recurrent glioblastoma. *JCO* 2020;38:2534.
8. Hu Q, Ye X, Qu X, et al. Discovery of a novel IL-15 based protein with improved developability and efficacy for cancer immunotherapy. *Sci Rep* 2018;8:7675.
9. Hewitt SL, Bai A, Bailey D, et al. Durable anticancer immunity from intratumoral administration of IL-23, IL-36Γ, and Ox40L mRNAs. *Sci Transl Med* 2019;11.
10. Ribas A, Medina T, Kummar S, et al. SD-101 in combination with pembrolizumab in advanced melanoma: results of a phase IB, multicenter study. *Cancer Discov* 2018;8:1250:1250–7:.
11. Rizell M, Sternby Eilard M, Andersson M, et al. Phase 1 trial with the cell-based immune primer Ilixadencel, alone, and combined with sorafenib, in advanced hepatocellular carcinoma. *Front Oncol* 2019;9:19.
12. Wu X, Wu Y, Ye H, et al. Interleukin-15 and cisplatin co-encapsulated thermosensitive polypeptide hydrogels for combined immuno-chemotherapy. *J Control Release* 2017;255:81–93.
13. Read TA, Smith A, Thomas J, et al. Intralesional PV-10 for the treatment of in-transit melanoma metastases—results of a prospective, non-randomized, single center study. *J Surg Oncol* 2018;117:579–87.
14. Spicer J, Marabelle A, Baurain J-F, et al. Safety, antitumor activity, and T-cell responses in a dose-ranging phase I trial of the oncolytic peptide LTX-315 in patients with solid tumors. *Clin Cancer Res* 2021;27:2755–63.
15. Pasquereau-Kotula E, Habault J, Kroemer G, et al. The anticancer peptide Rt53 induces Immunogenic cell death. *PLOS ONE* 2018;13:e0201220.
16. Boyle GM, D'Souza MMA, Pierce CJ, et al. Intra-lesional injection of the novel PKC activator EBC-46 rapidly ablates tumors in mouse models. *PLOS ONE* 2014;9:e108887.
17. Cullen JK, Boyle GM, Yap P-Y, et al. Activation of PKC supports the anticancer activity of tigilanol tiglate and related epoxytiglianes. *Sci Rep* 2021;11:207.
18. Colón-González F, Kazanietz MG. C1 domains exposed: from diacylglycerol binding to protein–protein interactions. *Biochim Biophys Acta* 2006;1761:827–37.
19. Barnett CME, Broit N, Yap P-Y, et al. Optimising Intratumoral treatment of head and neck squamous cell carcinoma models with the diterpene ester tigilanol tiglate. *Invest New Drugs* 2019;37:1–8.
20. De Ridder T, Ruppin M, Wheeless M, et al. Use of the intratumoural anticancer drug tigilanol tiglate in two horses. *Front Vet Sci* 2020;7:639.
21. De Ridder TR, Campbell JE, Burke-Schwarz C, et al. Randomized controlled clinical study evaluating the efficacy and safety of Intratumoral treatment of canine mast cell tumors with tigilanol tiglate (EBC-46). *J Vet Intern Med* 2021;35:415–29.
22. Panizza BJ, de Souza P, Cooper A, et al. Phase I dose-escalation study to determine the safety, tolerability, preliminary efficacy and pharmacokinetics of an Intratumoral injection of tigilanol tiglate (EBC-46). *EBioMedicine* 2019;50:433–41.

23 Brasaemle DL, Dolios G, Shapiro L, *et al*. Proteomic analysis of proteins associated with lipid droplets of basal and lipolytically stimulated 3T3-L1 adipocytes. *J Biol Chem* 2004;279:46835–42.

24 Zhang S, Wang Y, Cui L, *et al*. Morphologically and functionally distinct lipid droplet subpopulations. *Sci Rep* 2016;6:29539.

25 Le Saux CJ, Ho TC, Brumwell AM, *et al*. BCL-2 modulates Ire1Α activation to attenuate ER stress and pulmonary fibrosis. *Am J Respir Cell Mol Biol* 2024;70:247–58.

26 Fucikova J, Kepp O, Kasikova L, *et al*. Detection of Immunogenic cell death and its relevance for cancer therapy. *Cell Death Dis* 2020;11.

27 Garris CS, Arlauckas SP, Kohler RH, *et al*. Successful anti-PD-1 cancer immunotherapy requires T cell-dendritic cell crosstalk involving the cytokines IFN-Γ and IL-12. *Immunity* 2018;49:1148–61.

28 Hetz C, Papa FR. The unfolded protein response and cell fate control. *Mol Cell* 2018;69:169–81.

29 Callegari S, Dennerlein S. Sensing the stress: a role for the UPR(Mt) and UPR(Am) in the quality control of mitochondria. *Front Cell Dev Biol* 2018;6:31.

30 Urano F, Wang X, Bertolotti A, *et al*. Coupling of stress in the ER to activation of JNK protein kinases by transmembrane protein kinase Ire1. *Science* 2000;287:664–6.

31 Darling NJ, Cook SJ. The role of MAPK signalling pathways in the response to endoplasmic reticulum stress. *Biochim Biophys Acta* 2014;1843:2150–63.

32 Iurlaro R, Muñoz-Pinedo C. Cell death induced by endoplasmic reticulum stress. *FEBS J* 2016;283:2640–52.

33 Parker CG, Kuttruff CA, Galmozzi A, *et al*. Chemical proteomics identifies Slc25A20 as a functional target of the ingenol class of actinic keratosis drugs. *ACS Cent Sci* 2017;3:1276–85.

34 Halbleib K, Pesek K, Covino R, *et al*. Activation of the unfolded protein response by lipid bilayer stress. *Mol Cell* 2017;67:673–84.

35 Cho H, Stanzione F, Oak A, *et al*. Intrinsic structural features of the human Ire1Α transmembrane domain sense membrane lipid saturation. *Cell Rep* 2019;27:307–20.

36 Ertunc ME, Hotamisligil GS. Lipid signaling and lipotoxicity in metaflammation: indications for metabolic disease pathogenesis and treatment. *J Lipid Res* 2016;57:2099–114.

37 Yamamoto T, Endo J, Kataoka M, *et al*. Palmitate induces cardiomyocyte death via Inositol requiring enzyme-1 (ire1)-mediated signaling independent of X-box binding protein 1 (Xbp1). *Biochem Biophys Res Commun* 2020;526:122–7.

38 Ogata M, Hino S, Saito A, *et al*. Autophagy is activated for cell survival after endoplasmic reticulumstress. *Mol Cell Biol* 2006;26:9220–31.

39 Shen S, Niso-Santano M, Adjemian S, *et al*. Cytoplasmic stat3 represses autophagy by inhibiting PKR activity. *Mol Cell* 2012;48:667–80.

40 Kim B-J, Ryu S-W, Song B-J. JNK- and P38 kinase-mediated phosphorylation of BAX leads to its activation and mitochondrial translocation and to apoptosis of human hepatoma Hepg2 cells. *J Biol Chem* 2006;281:21256–65.

41 Donovan N, Becker EBE, Konishi Y, *et al*. JNK Phosphorylation and activation of BAD couples the stress-activated signaling pathway to the cell death machinery. *J Biol Chem* 2002;277:40944–9.

42 Morel C, Carlson SM, White FM, *et al*. Mcl-1 integrates the opposing actions of signaling pathways that mediate survival and apoptosis. *Mol Cell Biol* 2009;29:3845–52.

43 Galluzzi L, Vitale I, Aaronson SA, *et al*. Molecular mechanisms of cell death: recommendations of the nomenclature committee on cell death 2018. *Cell Death Differ* 2018;25:486–541.

44 Becerra A, Echeverría C, Varela D, *et al*. Transient receptor potential melastatin 4 inhibition prevents lipopolysaccharide-induced endothelial cell death. *Cardiovasc Res* 2011;91:677–84.

45 Ghosh S, Yang R, Duraki D, *et al*. Plasma membrane channel Trpm4 mediates Immunogenic therapy-induced necrosis. *Cancer Res* 2023;83:3115–30.

46 Nilius B, Prenen J, Tang J, *et al*. Regulation of the Ca2+ sensitivity of the nonselective cation channel Trpm4. *J Biol Chem* 2005;280:6423–33.

47 Marro BS, Zak J, Zavareh RB, *et al*. Discovery of small molecules for the reversal of T cell exhaustion. *Cell Rep* 2019;29:3293–302.

48 Bezu L, Sauvat A, Humeau J, *et al*. Eif2Α phosphorylation is pathognomonic for immunogenic cell death. *Cell Death Differ* 2018;25:1375–93.

49 Menger L, Vacchelli E, Adjemian S, *et al*. Cardiac glycosides exert anticancer effects by inducing Immunogenic cell death. *Sci Transl Med* 2012;4.

50 Yamazaki T, Wennerberg E, Hensler M, *et al*. LTX-315-enabled, radiotherapy-boosted Immunotherapeutic control of breast cancer by NK cells. *Oncoimmunology* 2021;10.